Pergamon

Int. J. Heat Mass Transfer. Vol. 38, No. 11, pp. 1975–1987, 1995

0017-9310/95 $9.50+0.00

0017-9310(94)00330-0

Convective heat transfer in a vertical anisotropic porous layer

G. DEGAN, P. VASSEUR† and E. BILGEN

Department of Mechanical Engineering, Ecole Polytechnique, University of Montreal, C.P. 6079, Succ. 'Centre-Ville', Montreal, P.Q., Canada H3C 3A7

(*Received* 11 *April* 1994 *and in final form* 12 *October* 1994)

Abstract—This paper summarizes an analytical and numerical study of natural convection in a fluid-saturated porous medium filled in a rectangular cavity. The porous medium is assumed to be both hydrodynamically and thermally anisotropic. The principal directions of the permeability are oriented in a direction that is oblique to the gravity vector, while those of thermal conductivity coincide with the horizontal and vertical coordinate axes. The side walls of the cavity are, respectively, heated and cooled by a constant heat flux while the horizontal walls are adiabatic. An analytical solution, valid for stratified flow in slender enclosures, is presented. Scale analysis is applied to predict the order of magnitudes involved in the boundary layer regime. Comparisons between the fully numerical and analytical solutions are presented for $A = 4$, $0 \leqslant R \leqslant 600$, $10^{-3} \leqslant k^* \leqslant 10^3$, $10^{-3} \leqslant K^* \leqslant 10^3$ and $0° \leqslant \theta \leqslant 180°$ where A, R, k^*, K^* and θ denote the enclosure aspect ratio, Rayleigh–Darcy number, anisotropic thermal conductivity ratio, anisotropic permeability ratio and the inclination angle of principal axes of the anisotropy in the permeability, respectively. It is found that the analytical solutions can faithfully predict the flow structure and heat transfer for a wide range of the governing parameters. The results indicate that a maximum (minimum) heat transfer rate can be obtained if the porous matrix is oriented with its the principal axis with higher permeability parallel (perpendicular) to the vertical direction. Also, it is found that a large thermal conductivity ratio causes a higher flow intensity but a lower heat transfer.

INTRODUCTION

Buoyancy-driven convection in fluid-saturated porous media has many applications. Prominent among these are insulation techniques, flows in soils, aquifers, petroleum extraction, storage of agricultural products, underground diffusion of contaminants and porous material regenerative heat exchangers. Due to its importance, a considerable amount of information already exists. The state of the art has been summarized in a recent book by Nield and Bejan [1].

Most of the previous studies have usually been concerned with homogeneous isotropic porous structures. Within the last few years, however, the effects of non-homogeneity and anisotropy in porous media have been investigated. The inclusion of more physical realism in the matrix properties of the medium is important for the accurate modeling of the anisotropic media. Anisotropy, which is generally a consequence of a preferential orientation or asymmetric geometry of the grain or fibers, is in fact encountered in numerous systems in industry and nature.

Available works on this topic are concerned mostly with the study of natural convection in horizontal anisotropic porous layers heated from below. The critical Rayleigh number for the onset of convection was first considered by Castinel and Combarnous [2], who conducted an experimental and theoretical investigation for a layer with impermeable boundaries. The effect of thermal anisotropy on the onset of motion was studied by Epherre [3]. Kvernvold and Tyvand [4] extended these analyses to supercritical finite-amplitude convection. McKibbin [5] conducted an extensive study on the effects of anisotropy on the convective stability of a porous layer. At the upper surface of the porous medium he considered boundary conditions sufficiently general to allow both impermeable and constant-pressure boundaries. Nielsen and Storesletten [6] analyzed two-dimensional convection in rectangular channels with the lateral walls and horizontal boundaries permeable and conducting. It was demonstrated that, as expected, the effect of conductivity of the walls is stabilizing. Tyvand and Storesletten [7] investigated the problem concerning the onset of convection in an anisotropic porous layer in which the principal axes were obliquely oriented to the gravity vector. As a result, new flow patterns with a tilted plane of motion or tilted lateral cell walls were obtained. Also, it was demonstrated that the critical Rayleigh number was always reduced when compared with a perpendicular or parallel orientation of fibers vs boundaries. The effect of anisotropy of thermal instability in a fluid-saturated porous medium subjected to an inclined temperature gradient of finite magnitude was analyzed by Parthiban and Patil [8] using the Galerkin technique. It was found that anisotropic medium is most stable while either the isotropic situation or the horizontally isotropic situation is the

†Author to whom correspondence should be addressed.

NOMENCLATURE

A	aspect ratio of the cavity, H/L
a, b, c	constants, equation (10)
C	dimensionless vertical temperature gradient
g	gravitational acceleration
H	height of the cavity
i', j'	Cartesian coordinates coincident with the principal axes
k'_x, k'_y	thermal conductivity
k^*	thermal conductivity ratio, k'_x/k'_y
$\bar{\bar{K}}'$	flow permeability tensor, defined in equation (4)
K'_m, K'_n	permeability
K^*	anisotropic permeability ratio, K'_m/K'_n
L	thickness of the cavity
Nu	Nusselt number, equation (43)
p'	pressure
R	Darcy–Rayleigh number, $K'_m g\beta L\Delta T'/\alpha'_y v$
t'	time
T	dimensionless temperature, $(T'-T'_c)/\Delta T'$
T'_c	reference temperature at the geometric center of the cavity
$\Delta T'$	characteristic temperature difference, $q'L/k'_y$
ΔT	dimensionless wall-to-wall temperature difference
$\mathbf{V}'$	seepage velocity
u, v	dimensionless velocities in x and y directions, $(u', v')L/\alpha'_y$
x, y	dimensionless cartesian coordinates, $(x', y')/L$.

Greek symbols

$\bar{\bar{\alpha}}'$	thermal diffusivity tensor, defined in equation (4)
β	coefficient of thermal expansion of the fluid
θ	inclination of the principal axes
δT	temperature difference between vertical boundaries
ΔT	characteristic temperature difference chosen in the definition of the Nusselt number
ΔT^*	temperature difference between horizontal boundaries
μ	dynamic viscosity of the fluid
v	kinematic viscosity of the fluid
ρ	fluid density
ψ	dimensionless stream function, ψ'/α'_y.

Superscripts

$'$	dimensional quantities.

Subscripts

C	at the geometry center of the cavity
max	maximum value
min	minimum value
0	reference state.

most unstable one depending on the horizontal Rayleigh number and anisotropy parameters. Recently, Xiaoli Zhang *et al.* [9] studied Benard convection in a cavity filled with an anisotropic porous medium where the principal axes are non-coincident with the gravity vector. Both the permeability ratio and inclination angle of the principal axes were found to have a strong influence on the system. The existence or the co-existence of four solution branches, at supercritical Rayleigh number, was demonstrated.

Natural convection heat transfer in anisotropic porous media heated and cooled from the sides has received less attention. Burns *et al.* [10] examined analytically the convective heat transfer in a vertical slot. Both isothermal and non-isothermal walls were considered. The results demonstrated the dependence of the Nusselt number on the anisotropic permeabilities. Poulikakos and Bejan [11] showed that the nonuniformity of permeability and thermal diffusivity can have a dominating effect on the overall heat transfer rate. Lai and Kulacki [12] considered convection in a rectangular cavity with a vertical permeable interface between two porous media. The effects of sublayer thickness ratio, permeability contrast and nonuniform conductivity on the flow and temperature fields within the layered structure were discussed. Hong *et al.* [13] examined analytically the effets of nonuniform permeability conditions on the natural convection from a vertical plate in porous media. It was found the nonhomogeneity in permeability near the solid wall results in a strong flow-channeling effect that significantly increased the heat transfer. Ni and Beckermann [14] studied numerically the natural convection flow and heat transfer in a vertical enclosure filled with homogeneous porous media that are both hydrodynamically and thermally anisotropic. When compared to isotropic porous media it was found that the Nusselt number was enhanced by a large permeability ratio and reduced by a low one. A large thermal conductivity ratio caused a smaller Nusselt number but a low thermal conductivity ratio had very little effect on the heat transfer pattern. The problem of natural convection in a vertical cylinder filled with anisotropic porous media was considered by Chang and Hsiao [15]. The effects of anisotropic permeability ratio, anisotropic thermal conductivity ratio, Rayleigh number and geometrical aspect ratio on the flow field and heat transfer were discussed.

The effect of an anisotropic permeability of arbitrary orientation on the convective heat transfer in a vertical cavity heated isothermally from the side was investigated numerically by Xiaoli Zhang [16]. It was found that the flow changes from a mild convection to a boundary layer regime as the orientation of the principal axis with higher permeability was changed from horizontal to vertical. Recently, Chang and Liu [17] studied numerically the effects of anisotropic permeabilities, thermal diffusivity and wall conduction on the convective heat transfer in a rectangular porous cavity. The results indicate that as the ratios of the thermal diffusivity of the walls to porous cavity increase, the average Nusselt numbers increase. Also, it was demonstrated that a critical value of the anisotropic thermal diffusivity ratio may exist such that the Nusselt number reaches a minimum. This critical value decreases with increasing value of the anisotropic permeability ratio.

The present paper is concerned with natural convection in a vertical cavity filled with a porous medium. The side walls of the cavity are, respectively, heated and cooled at constant heat flux while the top and bottom walls are adiabatic. The porous medium is anisotropic in permeability with its principal axes oriented in a direction that is oblique to the gravity vector. Also, the porous medium is assumed anisotropic in thermal conductivity with the principal directions of the effective thermal conductivities coinciding with the horizontal and vertical coordinate axes. An analytical solution, valid for cavities with high aspect ratio ($A \gg 1$) is derived on the basis of a parallel flow approximation. A numerical study of the same problem, obtained by solving the complete system of governing equations, is also conducted. The results presented here are relevant to proper understanding of the general flow and heat transfer characteristics in anisotropic porous media.

MATHEMATICAL FORMULATION

The physical model considered in this paper is shown in Fig. 1. A two-dimensional vertical rectangular enclosure of height H and width L is filled with a porous medium. The two end walls are insulated, while a uniform heat flux q' is applied along both side walls. The thermophysical properties of the fluid are assumed constant, except for the density in the buoyancy term in the momentum equations. The porous medium is saturated with a fluid that is in local thermodynamic equilibrium with the solid matrix. The porous medium is anisotropic in flow permeability and thermal conductivity. The longitudinal and transverse components of the permeability are denoted by K'_m and K'_n, respectively. The permeability is transversly isotropic, whereas the principal directions of the thermal conductivities (k'_x, k'_y) coincide with the horizontal and vertical coordinate axes.

Assuming that the flow is laminar and that the cavity is long enough in the third (transverse) direction to allow the system to be treated as a two-dimensional rectangular cavity, the equations gouverning the conservation of mass, momentum (generalized Darcy's law) and energy, can be written as follows [18]:

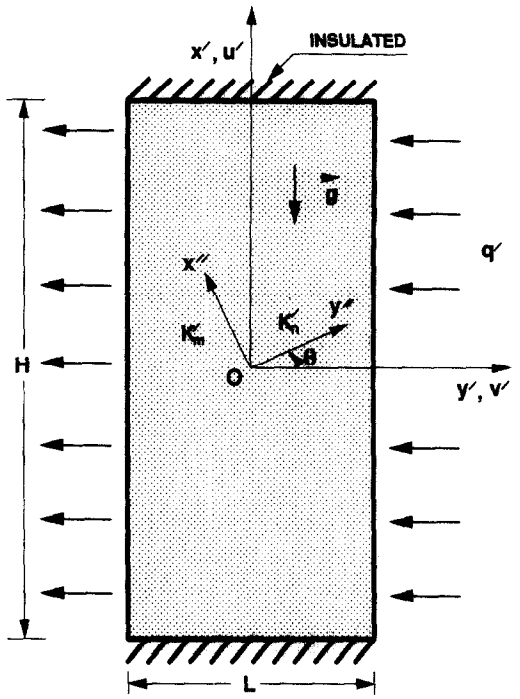

Fig. 1. Physical situation and coordinate system.

$$\nabla \cdot \mathbf{V}' = 0 \tag{1}$$

$$\mathbf{V}' = \frac{\bar{\bar{K}}'}{\mu}(-\nabla p' + \rho \mathbf{g}) \tag{2}$$

$$\frac{\partial T'}{\partial t'} + \nabla \cdot (\mathbf{V}' T' - \bar{\bar{\alpha}}' \nabla T') = 0 \tag{3}$$

where $\bar{\bar{K}}'$ and $\bar{\bar{\alpha}}'$ are the second order flow permeability and thermal diffusivity tensors defined, respectively, by

$$\bar{\bar{K}}' = \begin{bmatrix} K'_n & 0 \\ 0 & K'_m \end{bmatrix} \quad \bar{\bar{\alpha}}' = \begin{bmatrix} \alpha'_y & 0 \\ 0 & \alpha'_x \end{bmatrix} \tag{4}$$

$\mathbf{V}'$ is the superficial flow velocity, μ dynamic viscosity, p' pressure, ρ density, g gravitational acceleration, T' temperature, t' time and β coefficient of thermal expansion. It is noticed that the tensors $\bar{\bar{K}}'$ and $\bar{\bar{\alpha}}'$ are defined in the Cartesian frame of reference (O, Oy', Ox').

Using a linear equation of state and introducing the Boussinesq approximation

$$\rho = \rho_0[1 - \beta(T' - T'_0)] \tag{5}$$

with $L, \alpha'_y/L, q'L/k'_y$ and L^2/α'_y, as respective dimensional scales for length, velocity, temperature and time, the governing equations may be written in non-dimensional form as

$$\nabla \cdot \bar{\bar{K}} \nabla \psi - R \frac{\partial T}{\partial y} = 0 \tag{6}$$

$$\frac{\partial T}{\partial t} + \nabla \cdot (\nabla T - \bar{\bar{\alpha}} \nabla T) = 0 \tag{7}$$

where ψ is a dimensionless stream function defined as

$$u = \frac{\partial \psi}{\partial y}, \quad v = -\frac{\partial \psi}{\partial x} \tag{8}$$

such that equation (1) is identically satisfied, and

$$\left.\begin{aligned} R &= K'_m g \beta \Delta T' L / \alpha'_y \nu \\ \bar{\bar{K}} &= \begin{bmatrix} a & c \\ c & b \end{bmatrix} \quad \bar{\bar{\alpha}} = \begin{bmatrix} 1 & 0 \\ 0 & k^* \end{bmatrix} \end{aligned}\right\} \tag{9}$$

where

$$\left.\begin{aligned} a &= K^* \sin^2\theta + \cos^2\theta \\ b &= K^* \cos^2\theta + \sin^2\theta \\ c &= (1 - K^*) \sin\theta \cos\theta \\ K^* &= \frac{K'_m}{K'_n} \quad k^* = \frac{k'_x}{k'_y}. \end{aligned}\right\} \tag{10}$$

The non-dimensional boundary conditions over the walls of the enclosure are

$$y = \pm 1/2: \quad \psi = \frac{\partial \psi}{\partial y} = 0 \quad \frac{\partial T}{\partial y} = 1 \tag{11}$$

$$x = \pm A/2: \quad \psi = \frac{\partial \psi}{\partial x} = 0 \quad \frac{\partial T}{\partial x} = 0 \tag{12}$$

where $A = H/L$ is the cavity aspect ratio.

From the governing equations (6)–(7) and boundary conditions (11)–(12) it is seen that the present problem is governed by five dimensionless parameters: the aspect ratio of the cavity A, the Rayleigh number R, the thermal conductivity ratio k^*, the flow permeability ratio K^* and the angle of the principal axis θ.

DIMENSIONAL ANALYSIS

In the general case, the quantities of interest involved in the present problem are inter-related in a complicated way that would not allow estimation of their orders of magnitude by a scale analysis. However, at sufficiently high Rayleigh numbers the flow has a boundary layer flow structure for which an order of magnitude estimate can be derived on scaling grounds.

Let δy be the dimensionless thickness of the boundary layer on the vertical wall, and δu and δT be the velocity and temperature change across this layer. As discussed in the past by Bejan [19], in the case of a cavity heated from the sides at a constant heat flux we have to consider two temperature scales: namely δT the temperature change across the vertical wall and ΔT^* the temperature difference between the horizontal boundaries. These two temperature scales, although inter-related, are quite different.

From the thermal boundary conditions imposed along the vertical boundaries we have

$$\frac{\delta T}{\delta y} \sim 1 \tag{13}$$

while the Darcy's law and the energy equation require that

$$\delta u \sim \frac{R}{a} \delta T \tag{14}$$

$$\delta u C \sim \frac{\delta T}{\delta y^2} \tag{15}$$

where $C = \Delta T^*/A$ is the vertical temperature gradient in the core of the cavity.

From the above equations it is found that

$$\delta y \sim \left(\frac{R}{a}\right)^{-1/2} C^{-1/2} \tag{16}$$

$$\delta T \sim \left(\frac{R}{a}\right)^{-1/2} C^{-1/2} \tag{17}$$

$$\delta u \sim \left(\frac{R}{a}\right)^{1/2} C^{-1/2} \tag{18}$$

where the vertical temperature gradient C can be determined from the conservation of energy within a control volume of arbitrary height taken at the end of the cavity. It is readily found that

$$\delta u \delta T \delta y \sim k^* C. \tag{19}$$

Substituting equation (19) into equations (16)–(18) then gives

$$\delta y \sim \left(\frac{R}{a}\right)^{-2/5} k^{*1/5} \tag{20}$$

$$\delta T \sim \left(\frac{R}{a}\right)^{-2/5} k^{*1/5} \tag{21}$$

$$\delta u \sim \left(\frac{R}{a}\right)^{3/5} k^{*1/5} \tag{22}$$

$$C \sim \left(\frac{R}{a}\right)^{-1/5} k^{*-2/5}. \tag{23}$$

Let us consider now the case where the convection is strong enough for a horizontal boundary layer to develop along the upper and lower surfaces of the enclosure. Let δx be the thickness of these horizontal boundary layers, and δv and δT^* be the velocity and temperature changes, respectively. From the conservation of mass we have

$$\frac{\delta u}{\delta x} \sim \frac{\delta v}{\delta y} \tag{24}$$

while the Darcy's equation requires that

$$\frac{\delta v}{\delta x} \sim \frac{R}{b}\delta T. \tag{25}$$

From the conservation of energy we have

$$\delta u \delta T \delta y \sim k^* \frac{\delta T^*}{\delta x}. \tag{26}$$

These balances readily give

$$\delta x \sim a^{-3/10} b^{1/2} k^{*1/10} R^{-1/5} \tag{27}$$

$$\delta v \sim a^{1/10} b^{-1/2} k^{*3/10} R^{2/5} \tag{28}$$

$$\delta T^* \sim a^{-1/10} b^{1/2} k^{*-3/10} R^{-2/5}. \tag{29}$$

The above results can be summarized as follows:

$$u \sim R^{3/5} a^{-3/5} k^{*1/5} \tag{30}$$

$$v \sim R^{2/5} a^{1/10} b^{-1/2} k^{*3/10} \tag{31}$$

$$\delta T \sim R^{-2/5} a^{2/5} k^{*1/5} \tag{32}$$

$$C \sim R^{-1/5} a^{1/5} k^{*-2/5}. \tag{33}$$

The Nusselt number, which will be defined later by equation (43) is given by

$$Nu \sim R^{2/5} a^{-2/5} k^{*-1/5}. \tag{34}$$

The order of magnitudes predicted in the present section will be confirmed by resorting to more elaborate numerical and analytical analyses.

NUMERICAL SOLUTION

A finite difference procedure was used for numerical integration of the coupled transport and energy equations. The temperature distribution was obtained from the energy equation (7) using the Alternating Direction Implicit method (ADI). The first and second derivatives were approximated by central differences and the time derivative by a first-order forward difference. The finite-difference form of the equation was written in conservative form for the advective term, in order to preserve the conservative property. Using this temperature field, the stream function was determined from equation (6) by Successive Over-Relaxation (SOR) before returning to the energy equation. Integration in time was continued to steady state.

The rectangular domain was divided into a uniform mesh. Numerical tests, using various mesh sizes were done for the same conditions in order to determine the best compromise between accuracy of the results and computer time. Typical results in terms of ψ_C, the value of the stream function at the center of the cavity, and Nu are given in Table 1. Based on these results a mesh size 51×51 was adopted for most of the cases considered in this study.

With thermal boundary conditions of uniform heating, the unicellular convective motion becomes independent of aspect ratio A for large aspect ratios [20]. Other numerical tests, using various aspect ratios, A, were done while other conditions, including the mesh size (51×51), were maintained constant. Results are given in Table 2. It can be seen from the table that ψ_C and Nu converge very fast to an asymptotic value when A is increased from unity. The aspect ratio $A = 4$ was adopted for all the cases investigated.

APPROXIMATE ANALYTICAL SOLUTION

In this section an approximate solution, valid for a tall enclosure ($A \gg 1$), is presented. In this limit, as discussed in detail by Cormack *et al.* [21], Walker and Homsy [22], Vasseur *et al.* [20, 23, 24], and other authors, the flow velocity in the central part of the cavity, far from either end, can be assumed parallel and in the x-direction. Only the velocity component $u(y)$ in that direction exists such that $\psi(x, y) = \psi(y)$. Also the temperature field is the sum of a linearly varying longitudinal part and an unknown transverse direction so that $T = Cx + \zeta(y)$ where C is the temperature gradient in the x-direction. Substituting these approximations into equation (6) and the steady-state form of equation (7), we have

$$\frac{d^3\zeta}{dy^3} - \alpha^2 \frac{d\zeta}{dy} = 0 \tag{35}$$

and

Table 1. Effect of mesh on ψ_C and Nu for $A = 4$, $R = 100$, $k^* = 1$ and $K^* = 1$

$M \times N$	20×20	40×40	50×50	80×80	Analytical solution
ψ_C	2.348	2.331	2.328	2.324	2.320
Nu	3.132	3.143	3.144	3.147	3.149

Table 2. Effect of aspect ratio A on ψ_C and Nu for $R = 100$, $k^* = 1$ and $K^* = 1$

A	1	2	3	4	5	Analytical solution
ψ_C	2.193	2.368	2.336	2.328	2.328	2.320
Nu	2.571	3.106	3.145	3.144	3.144	3.149

$$\frac{d^2\zeta}{dy^2} = C\frac{d\psi}{dy}. \tag{36}$$

Boundary conditions in the y-direction are now

$$y = \pm 1/2: \quad \psi = 0 \quad \frac{d\zeta}{dy} = 1. \tag{37}$$

The thermal boundary conditions in the x-direction cannot be reproduced exactly with the parallel flow approximation. However, we can impose an equivalent energy flux condition

$$\int_{-1/2}^{1/2} \left(\frac{\partial\psi}{\partial y}T - \frac{\partial T}{\partial x}\right)dy = 0. \tag{38}$$

Solutions of equations (35) and (36) satisfying equation (37) are

$$\psi = \frac{1}{C}\left(\frac{\cosh \alpha y}{\cosh \alpha/2} - 1\right) \tag{39}$$

$$T = Cx + \frac{1}{\alpha}\frac{\sinh \alpha y}{\cosh \alpha/2} \tag{40}$$

where

$$\alpha^2 = \frac{RC}{a}. \tag{41}$$

The heat flux condition (38) becomes

$$C = \frac{1}{2k^*C}\frac{1}{\cosh^2 \alpha/2}\left(\frac{\sinh \alpha}{\alpha} - 1\right). \tag{42}$$

The temperature gradient C can be obtained for any combination of the controlling parameters R, K^*, k^* and θ by numerically solving the above transcendental equation. However, this is a much easier task than numerically solving the full set of equations given in equations (5)–(11).

The heat transfer across the cavity can be expressed in terms of a Nusselt number Nu defined as

$$Nu = \frac{q'}{\overline{\Delta T}}\frac{L}{k'_y} = \frac{1}{\Delta T} = \frac{\alpha}{2}\coth\frac{\alpha}{2} \tag{43}$$

where $\overline{\Delta T}$ is the actual wall-to-wall temperature difference. According to equation (40) ΔT varies linearly in x and for convenience was evaluated arbitrarily at the position $x = 0$.

In the boundary layer regime, i.e. when $R \gg 1$, it may be easily shown from equations (41) and (42) that

$$\alpha = R^{2/5}a^{-2/5}k^{*-1/5} \tag{44}$$

and

$$C = R^{-1/5}a^{1/5}k^{*-2/5} \tag{45}$$

such that equations (39), (40) and (43) reduce to

$$\psi = \sqrt{k^*\alpha}(e^{\alpha(y-1/2)} - 1) \tag{46}$$

$$T = \frac{x}{\sqrt{k^*\alpha}} + \frac{1}{\alpha}e^{\alpha(y-1/2)} \tag{47}$$

$$Nu = \frac{\alpha}{2}. \tag{48}$$

The asymptotic behavior of the equations presented above, for the boundary layer regime, is exactly what was predicted by the previous dimensional analysis, as can been seen from equations (23), (32) and (34). Also, the above equations coincide with those obtained by Bejan [19] and Vasseur *et al.* [20] for $k^* = K^* = 1$, i.e. the isotropic medium.

It is also of interest to consider the case for which $\alpha \to 0$, which occurs either when $R \to 0$ (pseudo-conduction regime) or when the vertical thermal stratification $C \to 0$. In this situation, equation (42) yields

$$\alpha \simeq \frac{R}{2\sqrt{3a}\sqrt{k^*}} \tag{49}$$

such that from equation (41) it is found that

$$C \simeq \frac{R}{12ak^*}. \tag{50}$$

From equations (39) and (43) it is readily found that the stream function at the center of the cavity ψ_C and Nu are, respectively, given by

$$\psi_C \simeq -\frac{1}{8}\frac{R}{a}\left[1 - \frac{5}{576}\frac{R^2}{a^2k^*}\right] \tag{51}$$

and

$$Nu \simeq 1 + \frac{R^2}{144a^2k^*}. \tag{52}$$

RESULTS AND DISCUSSION

In this section the effects of anisotropic permeability and thermal diffusivity on the temperature and flow fields will be discussed separately. The results of these effects on a system with isotropic thermal properties ($k^* = 1$) are presented first. Results with a focus on the effect of non-uniform conductivity will then follow.

(a) *Effects of anisotropic permeability*

Figure 2a–c illustrates the effects of the permeability ratio K^* on streamlines and isotherms for $R = 100$ and $\theta = 45°$. In all these graphs the increments between adjacent streamlines and isotherms are $\Delta\psi = \psi_{max}/10$ and $\Delta T = (T_{max} - T_{min})/10$ where ψ_{max} is the maximum value of the stream function and T_{max} and T_{min} the maximum and minimum values of the dimensionless temperature located at the upper right-hand corner and lower left-hand corner of the cavity respectively. In an isotropic medium ($K^* = 1$) the flow and temperature fields of Fig. 2a are similar to the results obtained in the past by Bejan [19] and Vasseur *et al.* [20]. The main features of the convective flow are that the vertical boundary layer thickness is constant and the core region is motionless. Also, the core region is linearly stratified with a constant vertical

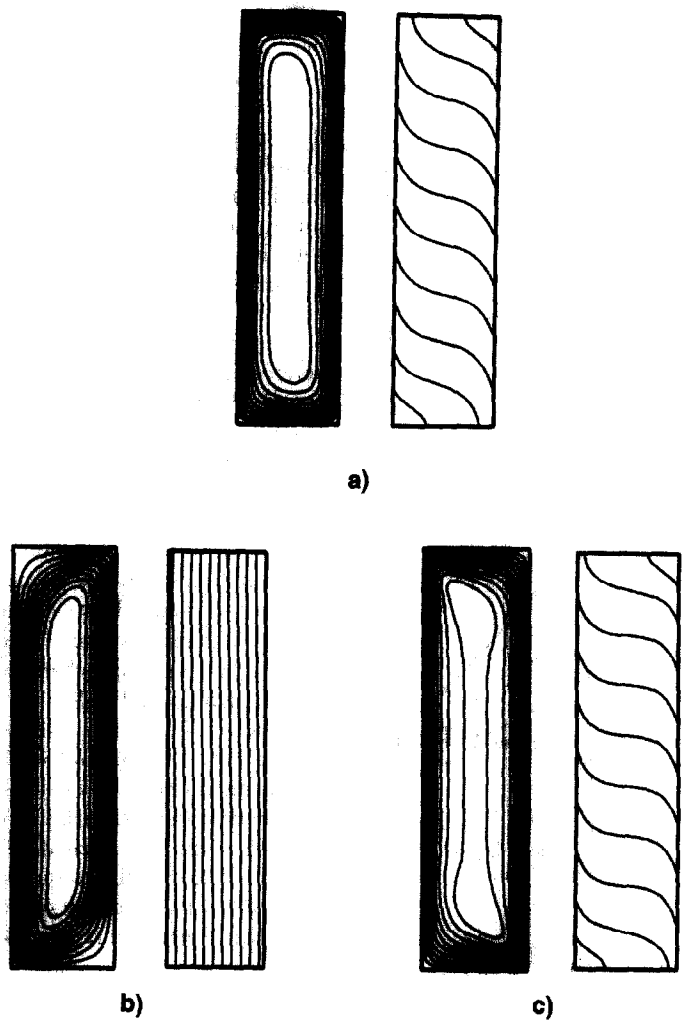

Fig. 2. Numerical solution for the flow and temperature fields, $R = 100$, $\theta = 45°$, $k^* = 1$ and (a) $K^* = 1$, $\psi_C = 2.328$, $T_{max} = 1.038$, $T_{min} = -1.038$; (b) $K^* = 10^3$, $\psi_C = 0.025$, $T_{max} = 0.528$, $T_{min} = -0.528$; (c) $K^* = 10^{-3}$, $\psi_C = 2.816$, $T_{max} = 0.913$, $T_{min} = -0.913$.

temperature gradient resulting in an altitude-independent temperature difference between the thermally active walls. Finally, due to the thermal boundary conditions considered here both the hydrodynamic and temperature boundary layer thicknesses are found to be equal. As $K^* > 1$, Fig. 2b shows that the strength of convection is smaller than that of the case of $K^* = 1$. This can be explained by the fact that an increase in K^* corresponds to a decrease in the permeability K_n', when other parameters are held constant, resulting in a weaker overall convective flow and heat transfer. Indeed, the vertical isotherms in Fig. 2b indicate that for $K^* = 10^3$ the convective motion inside the cavity is very weak ($\psi_C = 0.025$) and consequently the heat transfer mode is almost only due to the effects of pure conduction. Naturally, the reverse effects are observed as $K^* < 1$. Thus, Fig. 2d shows that, when $K^* = 10^{-3}$, both the flow and heat transfer have been promoted ($\psi_C = 2.816$) by an increase in the permeability K_n'. A similar trend has been reported in the past by Chang and Liu [17], while studying natural convection in a rectangular cavity heated isothermally from the sides and filled with an anisotropic medium having its principal axes aligned with the gravity vector ($\theta = 0°$).

The Nusselt number Nu and stream function at the center of the cavity ψ_C vs the permeability ratio K^* are presented in Fig. 3a and b, respectively, for $k^* = 1$, $\theta = 45°$ and various values of Rayleigh number R. In these graphs, the analytical results are continous lines. The numerical results, shown as blackened symbols, are seen to agree well despite the large range of parameters considered here. As expected, Fig. 3a and b indicates that, for a given value of K^*, the convective heat transfer increases as R is made larger. For a fixed value of R, both Nu and ψ_C tend asymptotically towards constant values as K^* is made small enough. This behavior is predicted, in the boundary layer regime, by equations (44), (46) and (48), from which it is predicted that $Nu \to (R/\cos^2\theta)^{2/5}/2$ and $\psi_C \to (R/\cos^2\theta)^{1/5}$ when $K^* \to 0$. These limits are indicated as dashed lines in Fig. 3a

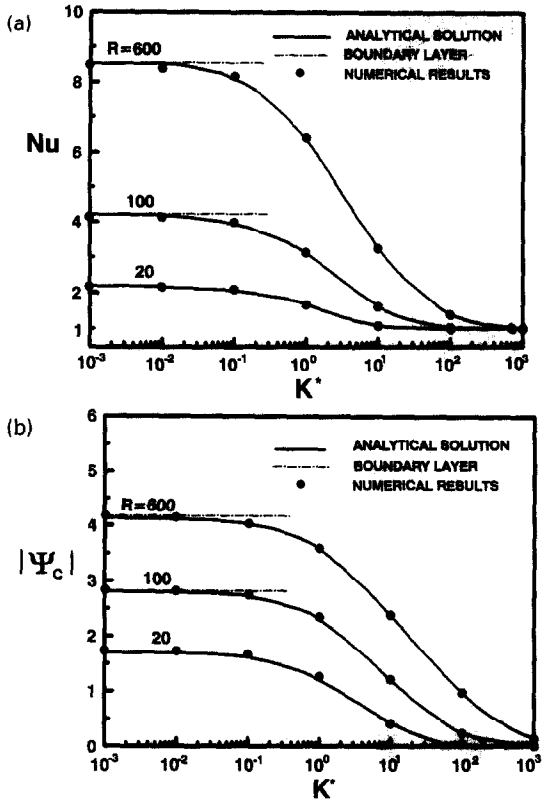

Fig. 3. Effect of permeability ratio K^* on (a) Nusselt number, (b) stream function at the center for $\theta = 45°$, $k^* = 1$ and various values of the Rayleigh number.

and b for $R = 100$ and 600. They are not given for $R = 20$, since for this situation, due to a relatively low Rayleigh number, a boundary layer regime is not reached. As discussed earlier, the convection becomes less and less vigorous as K^* is made larger. Thus, for each of the R considered in Fig. 3, the Nusselt number approaches the pure conduction regime, $Nu \to 1$ and $\psi_C \to 0$ as K^* is made large enough (see for instance Fig. 2b). The value of K^* necessary to reach the pure conduction regime depends upon R. For instance, for $R = 20$ pure conduction is reached when $K^* \simeq 10$ while for $R = 600$ the corresponding value is approximately $K^* \simeq 10^3$.

The influences of the anisotropy permeability ratio K^* and anisotropic orientation θ on the evolution of the streamlines and isotherms can be seen by comparing Figs. 2 and 4 corresponding to $R = 100$, $k^* = 1$, $K^* = 10^3$ and 10^{-3} and $\theta = 0, 45$ and 90°. The case of a porous medium with a large permeability ratio will be discussed first. For $\theta = 0°$, i.e. when the principal axes of anisotropy are aligned with respect to the gravity vector, it is observed from Fig. 4a that the buoyancy flow for $K^* = 10^3$ is considerably lower than that for $K^* = 1$ (Fig. 2a). Consequently the heat transfer is mostly by pure conduction, as indicated by the almost vertical isotherms of Fig. 4a. The resulting flow pattern is found to be similar to that obtained by Ni and Beckermann [14] for the case of a square cavity ($A = 1$) heated isothermally from the sides. Hence, the flow is seen to be channeled along the vertical walls, such that the hydrodynamic boundary layer is relatively thin. This phenomenon occurs even though the porous medium is homogeneous because the permeability in the vertical direction is much greater than that in the horizontal direction. The effect of the anisotropy orientation on flow and temperature distributions is depicted in Figs. 4a, 2b and 4c for $\theta = 0$, 45 and 90°, respectively. These figures clearly show that the strength of the flow circulation is reduced as the orientation of the principal axis with higher permeability is changed from vertical ($\theta = 0°$) to horizontal ($\theta = 90°$). Also, the velocity boundary layers observed along the vertical walls for $\theta = 0°$, Fig. 4a, have been destroyed upon increasing the orientation θ to 90° (Fig. 4c). For this situation the permeability in the horizontal direction is now much greater than that in the vertical direction thus spreading in the horizontal direction any nonuniformities in the vertically flowing fluid. However, due to the relatively low permeability in the vertical direction, the horizontally flowing fluid is strongly channeled along the two adiabatic horizontal end walls.

The case of a porous layer with a low anisotropic permeability ratio, $K^* = 10^{-3}$, will be now considered. For $\theta = 0°$, Fig. 4b shows that a reduction of the permeability ratio has very little influence on the strength of the flow circulation and the heat transfer patterns. The streamlines and isotherms shown in Fig. 4b for $K^* = 10^{-3}$ are very similar to those for $K^* = 1$ (Fig. 2a). Furthermore, Fig. 4b indicates that, not only is the flow pattern characterized by the presence of bone-shaped streamlines, but also the flow is found to be channeled along the upper and lower horizontal walls. Such a channeling effect has also been observed by Ni and Beckermann [14] in the case of square cavity heated isothermally from the sides. This channeling effect can be attributed to the relatively low permeability prevailing now in the vertical direction. Indeed, the thickness of the channeling flow is predicted from the previous dimensional analysis, equation (27), according to which δx is proportional to $\sqrt{K^* R^{-1/5}}$ when θ is zero and is thus likely to occur only for small values of K^*. As the anisotropy orientation θ is increased from 0 to 90° the resulting flow and temperature patterns are illustrated in Figs. 4b, 2c and 4d. For $\theta = 45°$, Fig. 2c indicates that, due to the relatively high permeability K'_m, the flow in the end regions of the cavity is directed towards the upper left corner and the lower right one respectively. The flow in the central part of the cavity remains nevertheless essentially parallel. However, as the anisotropy orientation θ is increased further, the distorsion of the flow in the end regions spreads progressively in the core region. As a result, the parallelism of the flow within the cavity is progressively destroyed, as illustrated in Fig. 4d for $\theta = 90°$. Also this figure indicates the existence of an extremely thin vertical boundary layer. For this reason a poor agreement was observed

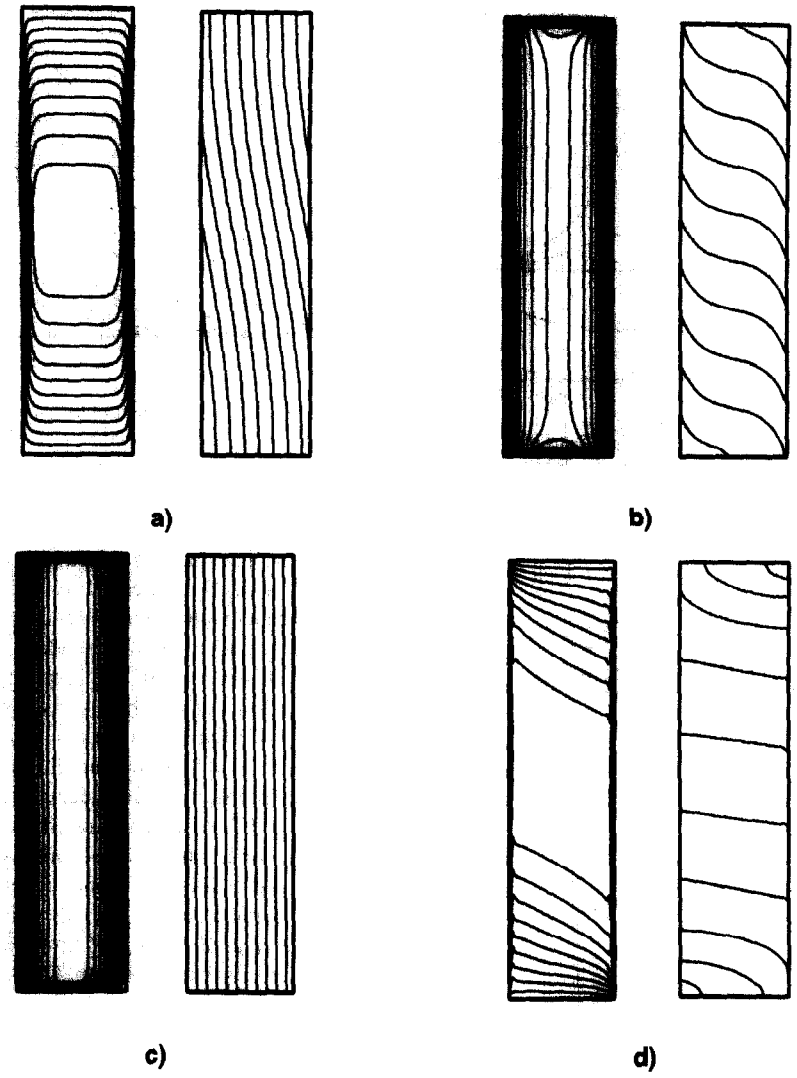

Fig. 4. Numerical solution for the flow and temperature fields, $R = 100$, $k^* = 1$ and (a) $\theta = 0°$, $K^* = 10^3$, $\psi_C = 0.195$, $T_{max} = 0.724$, $T_{min} = -0.724$; (b) $\theta = 0°$, $K^* = 10^{-3}$, $\psi_C = 2.330$, $T_{max} = 0.964$, $T_{min} = -0.964$; (c) $\theta = 90°$, $K^* = 10^3$, $\psi_C = 0.012$, $T_{max} = 0.515$, $T_{min} = -0.515$; (d) $\theta = 90°$, $K^* = 10^{-3}$, $\psi_C = 6.543$, $T_{max} = 0.589$, $T_{min} = -0.653$.

between these numerical results and the present analytical solution.

The influence of the anisotropy orientation θ on Nu and ψ_C are presented in Fig. 5a and b, respectively, for $R = 20$ and various values of K^*. In an isotropic medium ($K^* = 1$) both Nu and ψ_C are independent of θ, as can be expected. In general, a symmetry of the results with respect to $\theta = 90°$ is observed in Fig. 5. This follows from the fact that it can be shown, from the governing equations (6) and (7) and boundary conditions (11)–(12) that if $\psi(x, y)$ and $T(x, y)$ are solutions for R, K^*, k^* and θ then $\psi(x, 1-y)$ are solutions for R, K^*, k^* and $\pi-\theta$. We can therefore limit the discussion to $0 \leqslant \theta \leqslant 90°$. Figure 5a and b also indicates that for $K^* < 1$ both Nu and ψ_C are minimum at $\theta = 0°$, for which the permeability in the vertical direction is minimum, but maximum at $\theta = 90°$ for which the permeability in the vertical direction is maximum. The inverse is observed for $K^* > 1$ for which the convective heat transfer is now maximum at $\theta = 0°$ and minimum at $\theta = 90°$. This behavior can easily be demonstrated from the analytical solution, at least in the boundary layer regime. Taking the first derivative of Nu with respect to θ, equations (48) and (44), and making the result equal to zero it is readily found that $(K^* - 1) \sin 2\theta = 0$ such that a maxima or a minima occurs for $\theta = 0°$ and 90°. From the second derivative it is found that $d^2Nu/d\theta^2 = \pm R^{2/5}(K^* - 1)/k^{*1/5}$ when $\theta = 0°$ and 90°, respectively. Thus, when $K^* > 1 (K^* < 1)$ Nu is maximum (minimum) at $\theta = 0°$ and minimum (maximum) at $\theta = 90°$. It follows from these results that a maximum (minimum) convective heat transfer is reached when the orientation of the principal axis with higher permeability of the anisotropic porous medium is parallel (perpendicular) to the gravity.

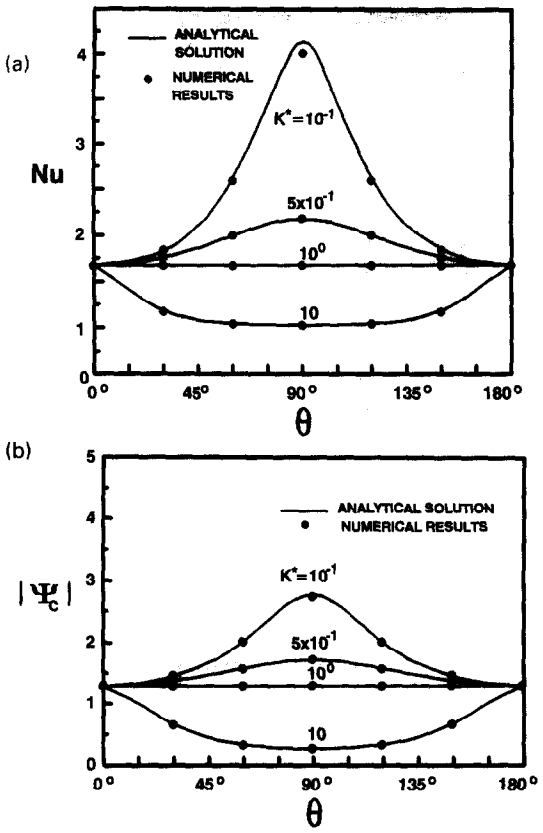

Fig. 5. Effect of anisotropy orientation angle θ on (a) Nusselt number, (b) stream function at the center for $R = 20$, $k^* = 1$ and various values of permeability ratio.

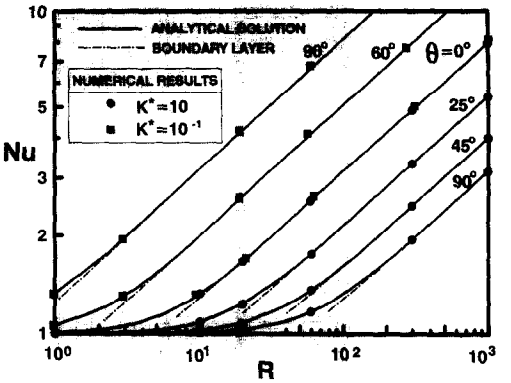

Fig. 6. Effect of the Rayleigh number on the Nusselt number for $k^* = 1$, $K^* = 0.1$ and 10 and various values of anisotropy orientation angle.

These results are qualitatively similar to those obtained numerically by Xiaoli Zhang [16], while studying the effect of an anisotropic permeability of arbitrary orientation on the convective heat transfer in a vertical porous cavity heated isothermally from the side.

The above results can be used to minimize the loss of heat through a vertical layer and have thus applications in insulation techniques. According to Kvernvold and Tyvand [4] the class of porous materials defined by $0 < K^* < 1$ may be interpreted as a medium composed of parallel fibers. Figure 5a shows that the heat transport is minimum for horizontal fibers and maximum when the same fibers are turned vertically. The class of porous materials defined by $K^* > 1$ may be interpreted as a medium composed of perforated parallel plates. For this situation the Nusselt number is minimum for horizontal plates and maximum for vertical plates. Thus, it is concluded that the anisotropic medium which gives the best insulation is a medium with as small a vertical permeability as possible. A similar conclusion has been reached by Kvernvold and Tyvand [4] while studying free thermal convection in a horizontal anisotropic porous layer heated from below.

Figure 6 shows Nu vs R for selected values of the anisotropy orientation θ and $K^* = 10^{-1}$ and 10, respectively. The analytical solution, equation (46), is compared with the numerical results and is observed to be in excellent agreement. When $\theta = 0°$, the Nusselt number is found to be independent of K^* (see also Fig. 5a). This is only in the limit of a parallel flow approximation, for which it is easily seen from equations (41)–(43) that $a = 1$ for $\theta = 0°$ and Nu becomes independent of K^*. However, in general, when the flow is not parallel Nu does depend upon the anisotropic ratio K^*, as demonstrated by Ni and Bekermann [14] for a square enclosure ($A = 1$). Also, as discussed earlier it is seen from Fig. 6 that for $K^* < 1$ the heat transfer is enhanced as the anisotropy orientation is increased from zero towards 90° while the reverse effect is observed for $K^* > 1$. The Nusselt number predicted for the boundary layer regime equations (48), is included as dashed lines in Fig. 6 for comparison. The start of the boundary layer regime is strongly dependent on K^* and θ. For instance for $\theta = 90°$ the boundary layer regime starts at $R \simeq 2$ for $K^* = 10^{-1}$ whereas it starts only at $R \simeq 200$ for $K^* = 10$.

(b) *Effects of anisotropic thermal conductivity*

Figure 7a and b shows the streamlines and isotherms obtained numerically for $R = 100$, $K^* = 1$ and $k^* = 10^3$ and 10^{-3}, respectively. The flow and temperature patterns corresponding to a porous medium with an isotropic thermal conductivity ($k^* = 1$) are depicted in Fig. 2a. For $k^* = 10^3$ the isotherms in Fig. 7a are vertical, indicating that the heat transfer through the cavity is by pure conduction only. The absence of temperature gradients in the x-direction is due to the fact that the thermal conductivity in that direction is much higher than in the y-direction ($k^* \gg 1$). The resulting flow pattern has lost the boundary layer regime observed in Fig. 2a for $k^* = 1$ even though the flow intensity is now approximately five times higher. Despite the strong convective circulation within the porous layer, the flow pattern of Fig. 7a is rather typical of natural convection at a much lower Rayleigh number. A similar trend has

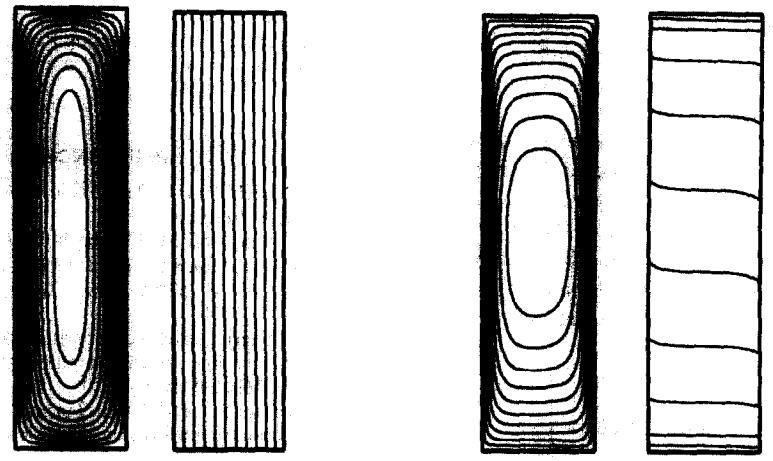

Fig. 7. Numerical solution for the flow and temperature fields, $R = 100$, $K^* = 1$, $\theta = 0°$ and (a) $k^* = 10^3$, $\psi_C = 11.598$, $T_{max} = 0.477$, $T_{min} = -0.477$; (b) $k^* = 10^{-3}$, $\psi_C = 0.901$, $T_{max} = 4.476$, $T_{min} = -4.476$.

been reported by Ni and Beckermann [14] while studying the effect of a large k^* on the convective flow within a square enclosure heated isothermally from the sides. However, it was reported by these authors that a low thermal conductivity ratio ($k^* \ll 1$) had very little influence on the flow and heat transfer patterns when compared with the isotropic situation ($k^* = 1$). This result is not in agreement with the findings of the present study where the streamlines and isotherms obtained for $k^* = 10^{-3}$ are shown in Fig. 7b. As it can be seen the isotherms are now considerably more horizontal than for $k^* = 1$ (Fig. 2a). This is expected since when k^* is small the thermal conductivity is much higher in the horizontal direction than in the vertical one. The resulting temperature pattern consists in a thermally stratified core region giving rise to a flow ciculation approximatively two and a half times lower than for the isotropic situation ($k^* = 1$). Despite this relatively weak convective circulation a boundary flow is observed to occur near the thermally active walls.

The effect of thermal conductivity ratio on the Nusselt number and stream function at the center of the cavity is depicted in Fig. 8a and b, respectively, for $K^* = 1$ and $R = 20$, 100 and 200. Figure 8a shows that, for a given R, Nu approaches unity as the value of k^* is made large enough. This is predicted by the present theory, equations (49)–(52), which shows that when k^* is large enough both C and α tend towards zero, independently of the value of R, such that the heat transfer is mostly by pure conduction ($Nu \to 1$). Naturally, the thermal conductivity ratio necessary to reach this situation increases with an increase of R. For instance it occurs when $k^* \simeq 10$ for $R = 20$ and $k^* \simeq 10^3$ for R = 200. In general, a Nusselt number approaching unity is associated with a pseudo-conduction regime, i.e. a very weak flow circulation within the cavity ($R \ll 1$). This is not the case in the present situation where the conductive heat transfer is not a consequence of a weak buoyancy force but rather is due to a large conductivity ratio. As a matter of fact, Fig. 8b shows that the strength of the convective flow ψ_C increases asymptotically with k^*, according to

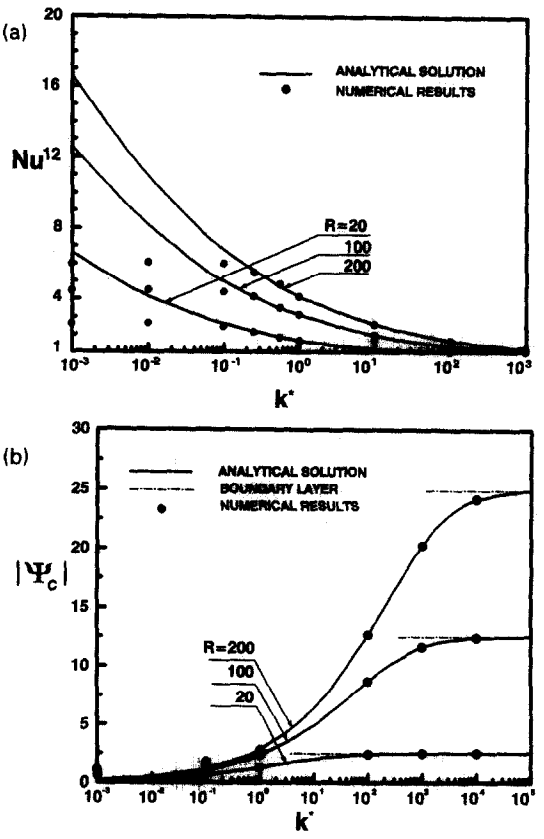

Fig. 8. Effect of thermal anisotropy ratio k^* on (a) Nusselt number, (b) stream function at the center for $K^* = 1$ and various values of the Rayleigh number.

equation (51), towards a maximum value $|\psi_C| = R/8$. Upon comparing the analytical solution with the numerical solution it is noticed that for $k^* > 1$ the agreement between both results is excellent. However, as the value of k^* is made smaller than unity the analytical Nusselt is seen to increase continuously while the numerical results tend towards a constant value that depends upon R. This deviation is due to the fact that, as illustrated by Fig. 7b, the convective flow within the cavity is not parallel and the analytical solution becomes invalid for this situation.

CONCLUSIONS

A study is made of natural convection heat transfer in a vertical porous cavity exposed to a constant heat flux. The porous medium is assumed to be both thermally and hydrodynamically anisotropic with the principal axes of anisotropic permeability inclined with respect to the gravity force. An analytical solution, valid for flow in slender enclosures, is derived on the basis of a parallel flow approximation while a finite difference method is used to numerically simulate the convective flows. Detailed results for the flow field, temperature distribution and heat transfer rates have been presented for comparison. From these results, the following remarks are in order.

(1) Both the permeability ratio and inclination angle of the principal axes have a strong influence on the thermal convection in anisotropic porous media.

(2) A large permeability ratio ($K^* > 1$) causes channeling of the flow near the vertical walls when $\theta = 0°$. As the anisotropic orientation angle is increased the strength of the convective flow is progressively annihilated. For $\theta = 90°$ the flow pattern consists in a very weak convective flow in the core of the cavity with very thin velocity boundary layers near the horizontal walls. Independent of θ, all Nusselt numbers approach unity in the limit $K^* \to \infty$.

(3) A small permeability ratio ($K^* < 1$) causes channeling of the flow near the horizontal walls when $\theta = 0°$. The strength of the flow circulation is promoted with increasing θ. The heat transfer is maximum at $\theta = 90°$ for which the parallelism of the flow is destroyed for large values of R.

(4) A maximum (minimum) heat transfer within the cavity is obtained when the porous matrix is oriented in such a way that the principal axis with higher permeability is parallel (perpendicular) to the vertical direction. Thus, the best possible insulation is reached when the principal axis with lower permeability is parallel to the gravity.

(5) Upon increasing the thermal conductivity ratio ($k^* > 1$) the convective induced flow is promoted but the Nusselt number approaches unity as k^* is made large enough. As the thermal conductivity ratio is decreased ($k^* < 1$) Nu tends asymptotically towards a constant value that depends upon R.

Acknowledgements—This work was supported in part by the Natural Sciences and Engineering Research Concil, Canada and jointly by the FCAR, Government of Quebec.

REFERENCES

1. D. A. Nield and A. Bejan, *Convection in Porous Media*. Springer, Berlin. (1992).
2. G. Castinel and M. Combarnous, Critère d'apparition de la convection naturelle dans une couche poreuse anisotrope, *C. R. Hebd. Seanc. Acad. Sci. Paris B* **B278**, 701–704 (1974).
3. J. F. Epherre, Critère d'apparition de la convection naturelle dans une couche poreuse anisotrope, *Rev. Gen. Therm.* **168**, 949–950 (1975).
4. O. Kvernvold and P. A. Tyvand, Nonlinear thermal convection in anisotropic porous media, *J. Fluid Mech.* **90**, 609–624, (1979).
5. R. McKibbin, Thermal convection in a porous layer: effects of anisotropy and surface boundary conditions, *Trans. Porous Media* **1**, 271–292 (1984).
6. T. Nilsen and L. Storesletten, An analytical study on natural convection in isotropic and anisotropic porous channels, *J. Heat Transfer* **112**, 396–401 (1990).
7. P. Tyvand and L. Storesletten, Onset of convection in a anisotropic porous medium with oblique principal axes, *J. Fluid Mech.* **226**, 371–382 (1991).
8. C. Parthiban and P. R. Patil, Effect of inclined temperature gradient on thermal instability in an anisotropic porous medium, *Wärme Stoffübertragung* **29**, 63–69 (1993).
9. Xiaoli Zang, T. H. Nguyen and R. Kahawita, Convection flow and heat transfer in an anisotropic porous layer with principal axes non-coincident with the gravity vector, ASME Winter Annual Meeting, New Orleans, Louisana, U.S.A. *Fundamentals of Natural Convection*, HTD-Vol. 264, pp. 79–86 (1993).
10. P. J. Burns, L. C. Chow and C. L. Tien, Convection in a vertical slot filled with porous insulation, *Int. J. Heat Mass Transfer* **120**, 919–926 (1977).
11. D. Poulikakos and A. Bejan, Natural convection in vertically and horizontally layered porous media heated from the side, *Int. J. Heat Mass Transfer* **26**, 1805–1814 (1983).
12. F. C. Lai and F. A. Kulacki, Natural convection across a vertical layered porous cavity, *Int. J. Heat Mass Transfer* **31**, 1247–1260 (1988).
13. J. J. Hong, Y. Yamada and C. L. Tien, Effects of non-Darcian and nonuniform porosity on vertical plate natural convection in porous media, *J. Heat Transfer* **109**, 356–362 (1987).
14. J. Ni and C. Beckermann, Natural convection in a vertical enclosure filled with anisotropic porous media, *J. Heat Transfer* **113**, 1033–1037 (1993).
15. W. J. Chang and C. F. Hsiao, Natural convection in a vertical cylinder filled with anisotropic porous media, *Int. J. Heat Mass Transfer* **36**, 361–367 (1993).
16. Xiaoli Zhang, Convective heat transfer in a vertical porous layer with anisotropic permeability, *Proc. 14th Canadian Congr. Applied Mechanics*, Vol. 2, pp. 579–580 (1993).
17. W. J. Chang and H. C. Liu, Natural convection in a finite wall rectangular cavity filled with an anisotropic porous medium, *Int. J. Heat Mass Transfer* **37**, 303–312 (1994).
18. J. Bear, *Dynamics of Fluids in Porous Media*. Dover Publications, New York (1972).
19. A. Bejan, The boundary layer regime in a porous layer with uniform heat flux from the side, *Int. J. Heat Mass Transfer* **26**, 1339–1346 (1983).
20. P. Vasseur, M. G. Satish and L. Robillard, Natural convection in a thin, inclined porous layer exposed to a

constant heat flux, *Int. J. Heat Mass Transfer* **30,** 537–549 (1987).
21. D. E. Cormack, L. G. Leal and J. Imberger, Natural convection in a shallow cavity with differentially heated end walls. Part 1, asymptotic theory, *J. Fluid Mech.* **65,** 209–230 (1974).
22. K. L. Walker and M. G. Homsy, Convection in a porous cavity, *J. Fluid Mech.* **87,** 449–474 (1978).
23. P. Vasseur, C. H. Wang and M. Sen, Thermal instability and natural convection in a fluid layer over a porous substrate, *Wärme Stoffübertragung* **24,** 337–347 (1989).
24. P. Vasseur and L. Robillard, The Brinkman model for natural convection in a porous layer: effects of non-uniform thermal gradient, *Int. J. Heat Mass Transfer* **26,** 1339–1346 (1993).